COMMUNICATION

ChemComm
www.rsc.org/chemcomm

Synthesis, characterization and optical properties of ordered macroporous organosilicas†

Zuocheng Zhou, Xiaoying Bao and X. S. Zhao*

Department of Chemical and Biomolecular Engineering, National University of Singapore, 10 Kent Ridge Crescent, Singapore 119260. E-mail: chezxs@nus.edu.sg; Fax: +65 67791936; Tel: +65 68744727

Received (in Cambridge, UK) 16th March 2004, Accepted 7th April 2004
First published as an Advance Article on the web 24th May 2004

Ordered macroporous organosilica materials with uniform pore size in the range of 0.2–1.35 μm have been fabricated by using self-assembled colloidal crystals as templates, and characterized with SEM, TGA, FTIR, MAS NMR, and optical reflectance spectrometry.

The combination of inorganic and organic properties at the atomic or molecular level in a composite material offers great potential in the development of multifunctional hybrid materials for emerging applications.[1] Organosilicas are a family of such hybrid materials that has been available for many years.[2] To broaden their application areas and to strengthen their application potentials, a great deal of recent research effort has been directed towards synthesis of ordered porous organosilicas including microporous and mesoporous materials.[3–5] However, organosilicas with ordered pores of micrometre size have not been available, yet they may afford unique properties for applications such as biosensors,[6] DNA analysis,[7] low-dielectric-constant interlayers,[8] and photonic bandgap materials.[9]

Template synthesis is a facile approach to macroporous materials with ordered pore structure.[10,11] Here we demonstrate, for the first time, the preparation of ordered macroporous organosilicas (OMOSs) by using self-assembled polystyrene (PS) spheres as the template. PS spheres of uniform size were fabricated into face-centered cubic (fcc) colloidal crystals with either a sedimentation or a flow-controlled vertical deposition (FCVD) method.[12] The voids between the spheres were infiltrated with silsesquioxanes, including 1,2-bis(triethoxysilyl)methane (BTEM), 1,2-bis(triethoxysilyl-)ethane (BTEE), and 1,2-bis(triethoxysilyl)ethylene (BTEEY). Prehydrolysis of some of the silsesquioxanes was carried out to enable complete infiltration of the voids. Removal of the PS spheres by organic-solvent washing produced OMOSs (see ESI for the details of the preparation†). The samples prepared from the three silsesquioxanes are designed as OMOS-BTEM, OMOS-BTEE, and OMOS-BTEEY, respectively.

Fig. 1 shows the scanning electron microscopy (SEM) images of the annealed PS colloidal crystal and the OMOS materials templated by the colloidal PS crystal. The fcc structure of the PS crystal is seen from Fig. 1a. It is also seen that the PS spheres were connected each other *via* small necks, which formed during the annealing process. These necks provided the transport channels during the removal of the template by solvent washing. They were also the originator of the small pores connecting the air holes of the resultant OMOSs shown in Fig. 1b–d. The air holes have a diameter of about 1.35 μm, which is fairly consistent with the diameter of the PS spheres (1.5 μm). The slightly smaller diameter of the holes than that of the PS spheres may be due to the condensation of hydroxyl groups of the organosilicate networks during the processes of removal of the PS spheres and drying. Nevertheless, the three OMOS samples all display a fcc structure, which can be observed from the (100), (111) and (110) facets, showing a successful structure replication from the PS template. By varying the diameters of the PS spheres, OMOSs with different pore sizes have been obtained (see the SEM images of Fig. 1d–f).

† Electronic supplementary information (ESI) available: experimental details for materials preparation and characterizations, TGA curves and FTIR spectra. See http://www.rsc.org/suppdata/cc/b4/b403922j/

To confirm the presence of the bridging organic groups, the samples were characterized by thermogravimetric analysis (TGA), solid-state ^{13}C and ^{29}Si cross-polarization (CP) magic-angle spinning (MAS) NMR spectroscopy, and FTIR spectroscopy.

Shown in Fig. S1 of the ESI are the derivative TGA (DrTGA) curves of the OMOS samples under nitrogen atmospheres, together with that of the PS spheres used as the template. The peak observed at about 70 °C on the OMOS samples corresponds to the loss of physically adsorbed water and other gaseous species. The very broad peak centered at about 200 °C is due to the loss of hydrogen-bonded water, as well as dehydroxylation of silanol groups. Because of the relatively neutral environment used during hydrolysis and condensation of the silsesquioxanes, incomplete condensation of silanol groups was not unexpected. From Fig. S1 it can be seen that the decomposition temperature of PS spheres is about 450 °C under the experimental conditions. Thus, the prominent peak observed at about 420 °C on the three OMOS samples can be assigned to the decomposition of the PS template. However, because the decomposition temperatures of methylene, ethylene, and ethenylene species organosilicas are in the range of 400–500 °C,[13–15] the assignment of the peak at 420 °C is not straightforward. Above 500 °C, some small broad peaks can be seen on the OMOS samples, which could be due to the elimination of organic species as well as further dehydrogenation of surface silanol groups.

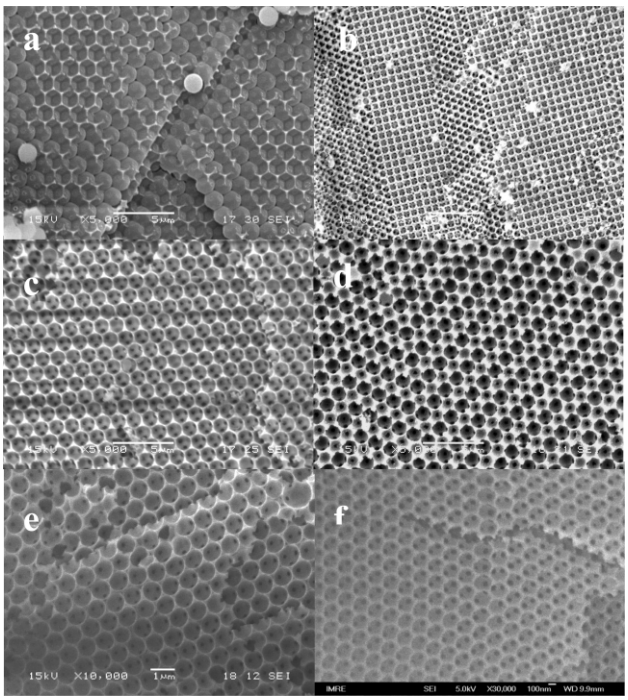

Fig. 1 SEM images of (a) colloidal crystal assembled from PS spheres of 1.5 μm after annealing at 110 °C for 10 min, (b) OMOS-BTEM observed along the (100) face, (c) OMOS-BTEEY observed along the (111) face, (d) OMOS-BTEE observed along the (110) face, (e) OMOS-BTEE with a pore diameter of 0.8 μm, and (f) OMOS-BTEE with a pore diameter of 0.2 μm.

DOI: 10.1039/b403922j

Nevertheless, the TGA data indicate that the organic species are thermally stable up to 400 °C.

Fig. S2 shows the FTIR spectra of the three OMOS samples. The broad absorption bands at 1000–1200 cm^{-1} demonstrate the formation of siloxane bonds. The presence of methylene, ethylene, and ethenylene bridges are evidenced by the appearances of the absorption bands at 1360 cm^{-1} for Si–CH_2–Si,[16] 1416 and 1270 cm^{-1} for Si–CH_2–CH_2–Si,[17] and 1580 and 1430 cm^{-1} for Si–C=C–Si moieties,[13,14] respectively. After solvent extraction three times, most of the PS had been removed as shown by the disappearance of the peaks due to PS.

The presence and chemical state of the organic species were further confirmed by the CP-MAS NMR spectra depicted in Fig. 2. The ^{13}C CP-MAS NMR spectra in Fig. 2A exhibit resonance peaks at 2, 4.5 and 146 ppm, which can be assigned to the carbons in the Si–CH_2–Si, Si–CH_2–CH_2–Si, and Si–CH=CH–Si groups,[13–15,18,19] respectively. The broad peaks observed from the ^{29}Si CP-MAS NMR spectra (Fig. 2B) at −59, −56 and −73 ppm correspond to the T_1, T_2 and T_3 Si sites of OMOS-BTEM, OMOS-BTEE, and OMOS-BTEEY,[13–15,18,19] respectively.

The optical properties of the OMOS materials were measured on a UV-3101PC UV–visible–near-infrared spectrophotometer. Fig. 3

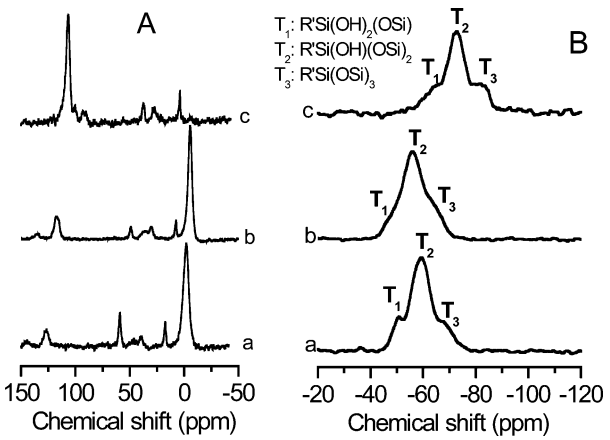

Fig. 2 (A) ^{13}C and (B) ^{29}Si CP-MAS NMR spectra of (a) OMOS-BTEM, (b) OMOS-BTEE, and (c) OMOS-BTEEY.

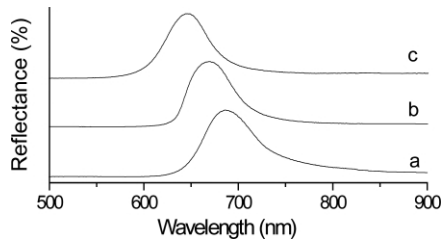

Fig. 3 Optical reflectance spectra of (a) OMOS-BTEE, (b) OMOS-BTEEY, (c) OMOS-BTEM.

Table 1 Peak positions of OMOSs and calculated values of the refractive indexes of OMOSs and organosilicas

Sample	Peak position/nm	n_a	n_o
OMOS-BTEE	686	1.106	1.406
OMOS-BTEEY	670	1.080	1.307
OMOS-BTEM	644	1.038	1.145

shows the reflectance spectra of the three OMOS films with a pore diameter of 380 nm. The observed peak positions are summarized in Table 1. The Bragg equation [eqn. (1)] was used to calculate the effective refractive indexes of the OMOS films and the organosilicas:

$$\lambda = 2dn_a \sin\theta \quad (1)$$

where λ_{max} is the wave position of peak, d is the lattice constant, n_a is the average refractive index of the OMOS films, θ is the angle of incident light. As the dominant surface of our samples is the (111) face, d can be calculated with eqn. (2).

$$d = d_{111} = (3/2)^{1/2} D \quad (2)$$

where D is the pore diameter of the OMOS films. The calculated results are included in Table 1 as well. From the values of n_a, the refractive indexes of the organosilica precursors (n_o) can be obtained from eqn. (3):

$$n_o = (n_a - n_{air} \times 74\%)/26\% \quad (3)$$

where n_{air} is the refractive index of air, which is 1. The calculated refractive indexes of the three organosilicas are 1.406, 1.307, and 1.145, which are less than that of the pure silica sample synthesized under the same conditions (1.431). This can be explained as the newly introduced Si–C bonds reducing the ionic polarization effect.[17] In addition, as the air holes in the OMOS films are arranged in a fcc structure with a volume ratio of 74%, the OMOS films possess a lower refractive index than the organosilicas, meaning the dielectric constant κ ($= n^2$) of the films is also lower than that of the organosilicas. By manipulating the sphere size of the OMOS films, their photonic bandgap can be tuned as well.

In conclusion, we have demonstrated the fabrication of ordered macroporous organosilica materials with tuning pore size and refractive index, which have high application potentials in catalysis, adsorption, and photonics.

Notes and references

1 C. Sanchez, G. J. de A. A. Soler-Illia, F. Ribot, T. Lalot, C. R. Mayer and V. Cabuil, *Chem. Mater.*, 2001, **13**, 3061.
2 D. A. Loy and K. J. Shea, *Chem. Rev.*, 1995, **95**, 1431.
3 A. P. Wight and M. E. Davis, *Chem. Rev.*, 2002, **102**, 3589.
4 A. Stein, B. J. Melde and R. C. Schroden, *Adv. Mater.*, 2000, **12**, 1403.
5 A. Sayari and S. Hamoudi, *Chem. Mater.*, 2001, **13**, 3151.
6 S. Howorka, S. Cheley and H. Bayley, *Nat. Biotechnol.*, 2001, **19**, 636.
7 J. Li, D. Stein, C. McMullan, D. Branton, M. J. Aziz and J. A. Golovchenko, *Nature*, 2001, **412**, 166.
8 W.-C. Wang, R. H. Vora, E.-T. Kang, K.-G. Neoh, C.-K. Ong and L.-F. Chen, *Adv. Mater.*, 2004, **16**, 54.
9 C. López, *Adv. Mater.*, 2003, **15**, 1679.
10 B. T. Holland, C. F. Blanford and A. Stein, *Science*, 1998, **281**, 538.
11 A. Imhof and D. J. Pine, *Nature*, 1997, **389**, 948.
12 Z. Zhou and X. S. Zhao, *Langmuir*, 2004, **20**, 1524.
13 T. Asefa, M. J. MacLachlan, N. Coombs and G. A. Ozin, *Nature*, 1999, **402**, 867.
14 T. Asefa, M. Kruk, M. J. MacLachlan, N. Coombs, H. Grondey, M. Jaroniec and G. A. Ozin, *J. Am. Chem. Soc.*, 2001, **123**, 8520.
15 T. Asefa, M. J. MacLachlan, H. Grondey, N. Coombs and G. A. Ozin, *Angew. Chem., Int. Ed.*, 2000, **39**, 1808.
16 C. Rau and W. Kulisch, *Thin Solid Films*, 1994, **249**, 28.
17 S. Sugahara, K. Usami and M. Matsumura, *Jpn. J. Appl. Phys.*, 1999, **38**, 1428.
18 B. J. Melde, B. T. Holland, C. F. Blandford and A. Stein, *Chem. Mater.*, 1999, **11**, 3302.
19 Y. Lu, H. Fan, N. Doke, D. A. Loy, R. A. Assink, D. A. LaVan and C. J. Brinker, *J. Am. Chem. Soc.*, 2000, **122**, 5258.